INDIAN JOURNAL OF SCIENCE AND TECHNOLOGY

RESEARCH ARTICLE

Classification of Long-Bone Fractures Using Modified Faster RCNN for X-Ray Images

Selin Vironicka[1]*, **J G R Sathiaseelan**[2]

1 Research Scholar, Department of Computer Science, Bishop Heber College (Affiliated to Bharathidasan University), Tiruchirappalli, Tamil Nadu, India
2 Associate Professor, Department of Computer Science, Bishop Heber College (Affiliated to Bharathidasan University), Tiruchirappalli, Tamil Nadu, India

OPEN ACCESS

Received: 17-08-2022
Accepted: 27-11-2022
Published: 06-01-2023

Citation: Vironicka S, Sathiaseelan JGR (2023) Classification of Long-Bone Fractures Using Modified Faster RCNN for X-Ray Images. Indian Journal of Science and Technology 16(1): 56-65. https://doi.org/10.17485/IJST/v16i1.1690

* **Corresponding author**.

mdselin933@gmail.com

Funding: None

Competing Interests: None

Published By Indian Society for Education and Environment (iSee)

ISSN
Print: 0974-6846
Electronic: 0974-5645

Abstract

Objectives: Methods in machine learning have been shown to be an essential tool for the diagnosis and treatment of disease. The scientists are constantly looking for new technology that might improve current clinical practise. One of the most well-liked study fields continues to be computerized bone fracture identification and categorization. Furthermore, identifying cracks and determining where they occur have been challenges for historically developed approaches for the long bone fracture method. **Methods:** We propose a new approach for automatic fracture detection in X-Ray images. This approach is built on top of two-stage fracture detection deep learning algorithm called Faster R-CNN with a major modification of using rotated bounding box. The described procedure is divided into four main steps: X-ray images are used to: I identify the bone contour; (ii) identify fracture-points or fractures; (iii) find a similar set of shapes that are compatible with the identification of cracks; and (iv) classify and thoroughly evaluate the fracture-type using bounding box. **Finding**: The resolution process uses the stretched numerical conventional line techniques (RDS), arcs, discrete curvature, and shape directory, among other mathematical characteristics of digital curves. We assessed the suggested model's performance in terms of classification and detection. We divide x-ray pictures of bone fractures into 2 groups, fracture and non-fracture, and we also use a rectangular box to identify the location of fractures. Besides, an additional benefit of rotated bounding box is that it can provide relative information on the orientation and length of fracture without the further segmentation and measurement step. **Novelty**: This study develops a new approach to automatically and accurately detect fractures in X-Ray images. The proposed approach is developed on the basis of Faster R-CNN algorithm with a major modification for the task of rotated bounding box prediction.

Keywords: Long bone; X-Ray images; Classification; Detection; Faster RCNN; Fracture; Non-Fracture; Types

1 Introduction

The use of computer-aided diagnosis (CAD) in the healthcare profession has been shown to be crucial for the management of diseases. There are numerous illness classification and detection methods available today. Machine learning, a subfield of artificial intelligence (AI), uses various systems to automatically identify, categorise, and forecast illness[(1)] . Deep learning, machine learning, and generalized imagery are currently the top AI technologies used in medicine[(2)]. Artificial neural networks with numerous layers are the foundation of deep learning models, which enhance efficiency[(3)]. X-rays, MRIs, CTs, and ultrasonic scanners are just a few of the diagnostic imaging devices that can be used to capture images of problems. But due to their accessibility and low cost, X-rays are the most often used method for diagnosing bone fractures[(4)]. Although there are several disorders that affect people in general, bone fractures are the most frequent[(5)]. A solid organ called bone exists in humans and guard's major organs like the pulse, lungs, and brain.

Approximately 206 bones in a body have various forms and configurations[(6)]. Bones come in a variety of shapes, including flat, short, long, sesamoid, and irregular. The femur is the largest bone, and the auditory ossicles are the smallest. A bone fracture is an everyday issue that only gets worse. A bone fracture happens when a bone is put under pressure that it cannot sustain. Long cracks, though, are frequent. A fracture might develop from a car crash, a bullet wound, or an injury sustained while participating in sports today[(7)]. Fractures come in a variety of forms, including typical, spiral, segmental, affected, torus, longitudinal, cohort, angled, and emerald sticks. Therefore, for management and therapy, it's crucial to identify bone fractures accurately and quickly[(8)]. The region of a bone fracture could be detected using a box using the older bone fracture diagnosis and grading techniques.

The suggested technique uses a to identify the fracture site in bone. In order to identify the advantages of each deep learning approach and attempt to define a generalised approach, Leonardo Tanzi classified bone fractures using a variety of deep learning approaches. Additionally, they outlined the critical elements that must be considered while attempting to achieve this goal and compared each study to our baseline. Deep learning, and in specifically the convolution neural network (CNN), has recently proved successful in the categorization of bone fractures that are on par with human performance[(9)]. To categorise fractured and normal bones, Yadav built the current model using deep neural networks. The tiny data set leads to an overfitting of the deep learning model. As a result, methods for enhancing data have been applied to expand the data collection. Three tests have been run to assess the model's effectiveness while employing the Softmax and Adam Optimizerm[(10)]. By employing straightforward images, Asma Alzaid seeks to evaluate the effectiveness of current classification methods. The effectiveness of systems that detect objects using 1 and 2 level designs was also assessed[(11)].

Egun Gülnur Beg study has three primary purposes: evaluating the dogs' development (Mission 1), courting cracks (Mission 2), and lastly, identifying dog long cracks (Task 3). Support vector machines (SVM), one of the most well-liked machine learning methods, is utilised for comparison. Accuracy and F1 score are used to evaluate each sub-performance. study's Various network architectures have been successful for every purpose[(12)]. A two-stage classification approach is suggested by Hadeer El-Saadawyv[(13)] for the identification of bone abnormalities and bone type identification. For all experiments, the only exception well before system is taken into account. For the system testing, two distinct strategies are used: One-view and multi-view techniques are the first two. The very first stage receives the improved images and assigns them to one of seven groups based on their location. The next step then receives the categorized bones and determines whether they are normal or pathological. All research has used the MURA dataset. Additionally, the SVM layer is substituted for the final layer of the network that was used.

A transfer learning Faster-RCNN deep-learning model with a major modification for the task of rotated bounding box prediction was developed in this study. This type of bounding box has advantages over other axis-align bounding box as it allows a better spatial constrain, such that the fracture is unique and fully contained in the bounding box. The idea underlying our approach is to take this advantage of rotated bounding box to minimize the ratio of background within the box and consequently provide a better prior spatial information to guide the fracture detection process. The four phases in our suggested strategy can identify and categorise a long-broken bone. In the initial stage, we immediately pre-processed the data, utilised Faster-RCNN for transfer learning, and then retrained the model's top layer. The developed model is finally assessed in terms of classification and detection. The frame determines whether or not there is a crack. The crack is accurately detected and classified continuously by the system. We test this models on 200 x-ray pictures of long bones from two fracture categories, fractured and non-fracture, in order to assess the suggested strategy. The results of the experiments show that the proposed system accurately and definitely identifies all sorts of fractures. Our suggested strategy has a 94.7% total accuracy for both classification and detection. With precise diagnosis and lower computing costs for fracture identification and tracking, an extremely coveted machine learning integrated approach. It assists physicians and specialists in coping with the physician's burden. First, we put forth a system that, in regards to classification quality and speed, is superior to conventional physicians at both detection and classification.

1.1 Fracture-Type Identification

There are various types of bone fractures, including simple, greenstick, comminute, and complicated fractures inFigure 2. A humble crack is a disruption in the bone that doesn't affect the skin above it in any unusual ways. In these situations, a bone may break into two pieces with only a slight displacement. A partial break in a bone known as a "greenstick fracture" occurs when one cross of the bone is shattered and the next part is curved. Mineralized and complex cracks both have many fragments.

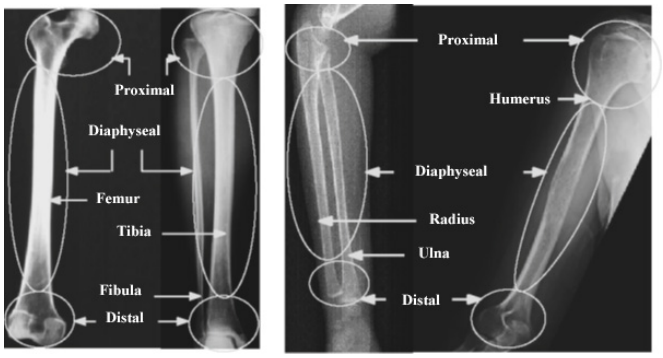

Fig 1. (a) Various part of tibia, femur, and fibula, (b) Various part of, radius, humours and ulna [(14)]

A bone that has been extensively broken, fractured, or broken into multiple pieces has suffered a mineralized fracture. The shattered bone may penetrate through the skin in a complex fracture. Figure 2 depicts the nature of break in various types of fractures; all long bones have a lengthy diaphyseal portion and proximal and distal regions that are rounded (Figure 1) [(14)]. As a result, both proximal and distal area injuries fall under different subclasses than diaphyseal region fractures. The suggested approach uses specific judgement criteria to categorise the fractured type for each region.

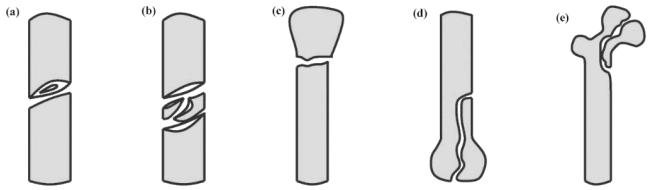

Fig 2. Types of fractures, (e) proximal (partial articular). (d) distal (partial articular), (c) proximal (extra-articular) (b) diaphyseal (complex) and (a) diaphyseal (simple)

1.2 Complex and wedge diaphyseal fracture

The long bone picture, we've applied the connected-component labelling (CCL) approach, which keeps track of how many line segments are present. Complex and wedge fractures have many fragmented components, according to investigations in the medical journals. While the primary pieces of a complicated fracture are totally isolated from one another, the main fragments of a wedge fracture maintain contact following reduction. Because of this, CCL analysis shows that simple or greenstick fractures have just one linked component, while wedge and complexity fractures have two or more related parts. The outer isothetic cover (OIC) for each of the broken mechanisms is determined using the isothetic-cover network approach after the CCL evaluation. The least isothetic polygon created on the backdrop grid, containing the digital object D, is covered by the OIC of the digital purpose D, executed on computer network H. Each grid point $((i, j) \in Z^2$ is many of g in this situation, where g denotes the digital plane grid size Z^2 and the $g \in Z^+$. The top-left pixel point $ms(x_0, y_0)$ of the object serves as the starting point for the building of an OIC, which finishes when the traverses around D's contour return to m s. Every single position on the OIC is calculated repeatedly up until the conclusion of the traversal (m n) coincides through ms.

The highest level, or g = 1, which is the precision used to create the digital X-ray image, yields the best approximate representation of a digital item. A closer representation of the actual contour will result from the use of greater values of g. When a bone is fractured by a blade, the major skeletal system is unaffected, and only minor movement occurs in the smaller bone fragments (see Figure 3 a). When g is set to 1 in this case, distinct OICs are formed for each of the little unconnected

fragments (Figure 3 b). The OIC, which encompasses the entire bone structure as well as the dislodged shrapnel in a book version, is created by a small uptick in grid size (g = 2). (as shown in Figure 3 c).

The misplaced splinters in complicated fractures are fully separated (see Figure 3 d). When a larger grid size (g = 3 or 4) is selected, the entire bone shape can be represented in a given OIC (see Figure 3 f). As a result, the suggested method uses the mesh density and CCL quantity for a given OIC to identify the wedge and complicated cracks.

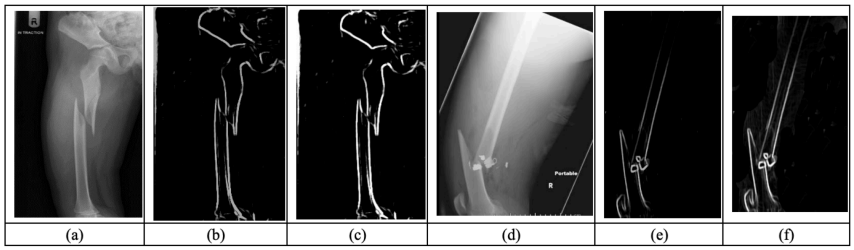

Fig 3. (a) long bone picture (wedge fracture), (b) and (e) grid size= 1 (c) and (f) grid size = 2, (d) long bone picture (complex fracture).

1.3 Simple diaphyseal fracture

There are three different varieties of simple fractures in the long bones' bony area: spiral, oblique, and transverse. An oblique crack features a sloped line of break that runs parallel to the axes of the bone. The suggested method classifies lines-of-break with gradients between 45° and 70° as belonging to the oblique group (see Figure 4 e). An axial transverse crack is one that occurs along the bone's long axis. Transverse fractures are defined as having an upright. All boundaries with a slope of less than 45 degrees are regarded as transverse fractures in the suggested technique (seeFigure 4 a).

When a bone sustains a spiral fracture, the shattered area spirals down the bone's long axis. Therefore, it is not enough to classify a spiral fracture based just on the slope of the line of break. The suggested solution looks at the contour curvature at the site of the crack to get around this issue. Contrary to what is seen in transverse and oblique cracks, the bending at the drop exhibits more frequently and discontinuous variations in a spiral cracked area. The suggested method analyses the relative-concavity (with = 5) of a 60-pixel window surrounding the break-point. This window has 30 predecessors and 30 descendants. An illustration of a spiral fracture is shown in Figure 4 c.

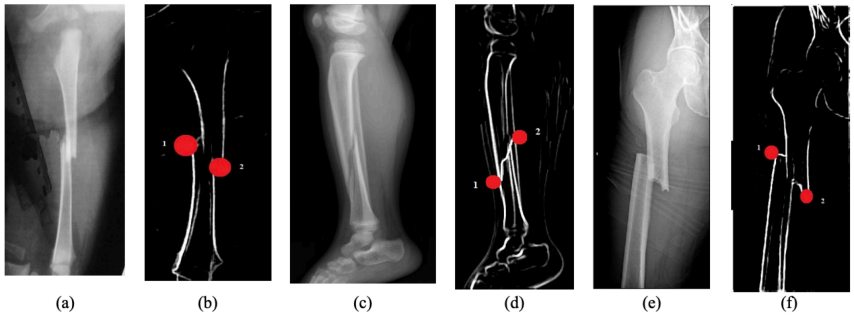

Fig 4. (a) long bone X ray picture (transverse fracture), (b) (d)and (f) with break line red part, (c) long bone X ray picture (spiral fracture), (e) long bone X ray picture (oblique fracture)

1.4 Proximal and distal region fracture

Image bones often have rounded proximal and distal parts. Based on how the ball's break affected it, fractures in these areas are categorised (the round shaped area). There are two different types of long bones' proximal regions: those with hinge joints (such as the tibia, femur, radius, and ulna) and those with ball-and-socket joints. While a proximate head with a free kick combined has a round pate preceded by a structural collar and a lengthy diaphysis area, the distal area and proximal top with curved lateral portions. The suggested system requires the characteristics of a digital circle to distinguish between a pate with a hinge-joint and one with a circular particle by analysing.

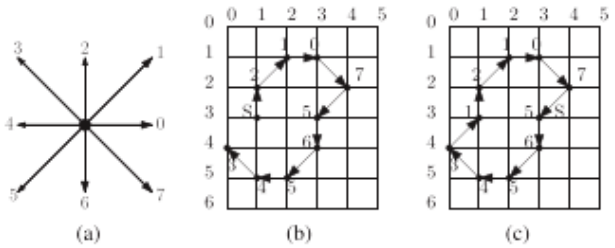

Fig 5. (a) 8-neighbor chain code for a net value (b) numerical arc (1, 3), (c) numerical arc (3, 3)

In the suggested strategy, we leverage the previously mentioned discontinuous bending notion to distinguish between different types of distal area cracks. We determine the bone's chain-code and extract the bone contour above the connection. The sphere shape of a distal head is suggested if the distinction between the two successive chain-codes is within the range of "0,1" and the moving in just the same orientation. A proximal head with a hinge-joint or a distal section of the bone are both indicated by an uneven character in the discrepancy.

2 Methodology

2.1 Exiting Method

The Faster-RCNN model was used to develop an automatic long bone fracture detection and classification system. The VGG-16 structure was chosen as the basic network in the suggested process to improve a feature map that will provide suggestions for crack area classification and detection.

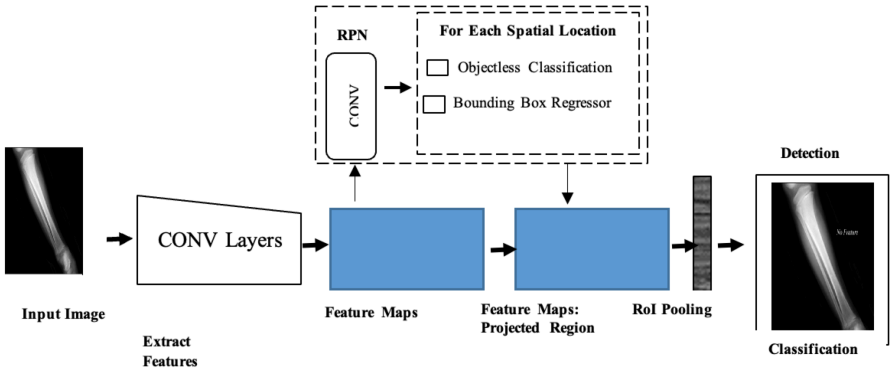

Fig 6. Block diagram of exiting method

2.1.1 CNN Network

Figure 6 illustrates the use of a transfer learning Faster R-CNN deep convolutional neural network at this level. The three neural networks that make up the Faster RCNN model are described here.

- Feature network
- Detection Network
- Region Proposal Network

a) Feature network

Typically, the term "Feature Network" refers to a system that eliminates several levels from classifier pictures during the last/top classification. This network's objective is to extract useful features from the photos. The outcome of this system retains the form and hierarchy of the main image.

b) Detection Network

The RPN and Feature Network provide input to the Detection Network, also known as the RCNN network, which then generates the very last class and bounding box. There are four densely integrated or dense levels in this structure. First layer is employed for classification, second layer is utilised for regression, and the final two levels are shared, stacking standard layers. To allow the boundaries squares to differentiate solely inside the RPN and the Recognition System require training, the characteristics are reduced in accordance with the bounding points.

c) Region Proposal Network

The RPN typically consists of a three-layer simple network. One component in particular feeds information into two other layers: the first layer for categorization and the third and second layers for regress bounding boxes. Bounding boxes, or regions of interest, are made using the RPN network. There is a good likelihood that there is an object in this area of interest. A number of bounding boxes identified by the pixel location of 2 vertical approaches, which have two sorts of data, are used to evaluate the performance of RPN. The possibilities for the likelihood that a fracture is depicted inside the box, or the box may be omitted, are 0, 1, and -1.

d) Training

In this phase, inception v2 (Version 2) networks are used to retrain the Faster RCNN's top layer. Training will keep going until the loss rate reaches 0.0005%. We trained the suggested technique to minimise convolution layer values, proposition region weights, and convolution layer filters using gradient descent stochastic (SGD). The variables are updated by stochastic gradient descent (SGD) for each instance of learning XCi) and label yCi).

$$\beta = \beta - \eta.\nabla\beta k(\beta; x^i; y^i) \tag{1}$$

Where β erudite rate and new knowledge rate are assumed. A procedure known as anchor boxes initially generates a number of bounding boxes before using them to train the RPN. An anchor is a single "pixel" created from a feature picture. The group of pixels in the primary picture's rectangular box known as an anchor box. On the segmentation process, the anchors box is evenly distributed along the X- and Y-axis measurements. A scalar form rather than the entire feature vector alone is the source needed to produce an anchor box first from information generating layer. Depending on every anchor, multiple rectangle boxes of various dimensions and shapes are generated. Normally, 9 boxes with a 3*3 size contents each box are made.

Technique known as Non-Maximum Suppression (NMS) was used during the initial stage of decrease. Boxes that overlay adjacent boxes with higher values are removed by NMS. The classification and detection threshold was set at 0.5. In the learning phase, close to 2,000 boxes are acquired. These boxes, together with their results, are sent directly to the Detection Network during the system testing. When moving to the classifier by filtering to about 256, the two thousand boxes are once again reduced throughout the training phase. IOUs are obtained from all anticipated boxes as well as regression coefficients boxes when we build RPN labels (such as forefront, backgrounds, and ignores). The IOUs are utilized to produce the labelling, which can be either fracture or normal. In addition, 256 boxes are produced, each of which includes an area of interest in both the background and foreground.

$$IoU = \frac{area\_overlap}{area\_union} \tag{2}$$

Cross-entropy is calculated by disregarding the boxes with -1 values. The bounding box is generated using an RPN network, which is then scaled to fit all around lengthy bone defects. The regressive anchoring box refers to this. In order to do this, a fracture must be identified and diagnosed. Losses must be recovered using backpropagation, and calculations for training must be made it after every stage. The expected anchoring box and regression coefficients box's central pixel are used to calculate a routing path, which is then normalised by size for the anchoring box.

The LI smooth expression is used to compute the depreciation. It is impossible for O to distinguish the usual loss of LI. By employing a loss of L2 past O, smooth loss of Ll gets around this. named sigma and assigned an L2 loss intensity of blew.

$$abs\,(N) < \frac{1}{S^2} \tag{3}$$

$$L = \frac{(d \times S)^2}{2} \tag{4}$$

Else

$$L = abs\,(d) - \frac{1}{(2 * S)^2} \tag{5}$$

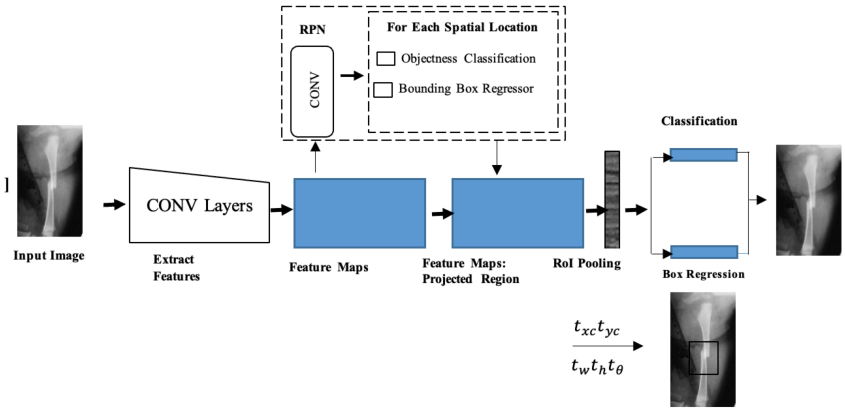

Fig 7. Block diagram of Proposed method

2.2 Proposed Work

Practically identical tasks are performed by RPN and R-CNN, although in varied contexts. As an illustration, they make improvements to the bounding box coordinates where a fracture is expected to stop in order to better match the shape of the fracture. The two differ in that RPN utilizes the whole features map created from the image data, whereas RCNN only uses a select few part areas in the feature maps matching to suggestion boxes for final bounding box estimates. The following sections will go over the adjustments within of each component required for rotating bounding box estimations.

Before delving into the specifics of the Faster R-CNN, it is useful to list the methods of rotational bounding box and anchor box. As was already mentioned, orientated rectangular boxes will be used to detect fractures. In order to compensate for box orientation, a further parameter of angle (0) is introduced for this bounding box description in addition to the four features typical of centre point coordinates (xc, ye), width (w), and height (h). This angle, which ranges from -90° to 90°, is specified as the angle between the bigger side of the bounding box and the positively vertical axis. It is also important to note that the bounding box's width is indeed smaller than its height. Anchor boxes are a collection of already-defined, rotating bounding boxes that have a specific scale, aspect ratio, and angle. They are evenly dispersed around the picture and will serve as examples when the RPN stage generates proposal boxes.

The following equations (6) through (10) will be used to determine the offset value between the allocated anchor boxes and the ground truth box. The scale-invariant shift between centre coordinates and the log-space height-width shift is shown in the (6) to (9) equations. The rotating angle is also shown in radian directions in the tenth equation. The branching or regressive will develop the ability to forecast those coordinates. Later, an anchor box will be transformed using the projected offset amounts.

$$t_x = ((x - x_a)/w_a \tag{6}$$

$$t_y = ((y - y_a)/h_a \tag{7}$$

$$t_w = bg(w/w_a) \tag{8}$$

$$t_h = bg(h/h_a) \tag{9}$$

$$t_\theta = (\theta - \theta_a) \times \frac{\pi}{180} \tag{10}$$

Where x_a, y_a w_a, h_a, and θ_a are x,y centre co-ordinates, width and height orientation of anchor box respectively. RPN only provides coarse bounding boxes that might contain fracture, while having a bounding box regression branch. The main cause is because RPN must employ high-variance anchor boxes in order to forecast prospective boxes.

2.3 Evolution

The model is assessed at these step-in terms of classification and detection.

2.3.1 Detection

A bounding box is also made around the crack in order to locate the fracture's location from the original x-ray picture.

2.3.2 Classification

Quality assessment matrices were utilised to categorise x-ray images as having a crack or not having a fracture.

2.3.3 Performance Matrices

Table 1. Classification performance metrics (P-Positive, N-Negative)

Predicted Class				
		P	**N**	
Actual Positive	**P**	T- Pos(TP)	F-Neg (FN)	Sensitivity (Recall) $\frac{TP}{(TP+FN)}$
	N	F-Pos(FP)	T-Neg (TN)	Specificity $\frac{TN}{(TN+FN)}$
		Precision $\frac{TP}{(TP+FP)}$	Neg-Predictive Value $\frac{TN}{(TN+FN)}$	Accuracy $\frac{TP+TN}{(TP+TN+FP+FN)}$

The framework depicts the crack one last time at this phase and creates a bounding box round the. Over an intermediary layer, Convolutional layers, and a Feature Map layer, the picture is sent to pre-trained CNN. From these layers, we feature extracted that we then use in the following section. The features that CNN generated were then employed by an Object Proposals Network (RPN) layer to identify the crack with a bounding box. We apply ROI (Region of Interest) pooling and record the characteristics that connect to an element into a vector that use the bounding boxes of interacting components and the features recovered by CNN. After classifying the input image as having a fracture or not, the R-CNN component modifies the bounding box's dimensions.

3 Results and Discussion

3.1 Dataset

The 200 x-ray pictures of patient long bone fractures make up the data utilized in this study, which was compiled using data gathered from the Rajiv Gandhi government General Hospital in Chennai. Eighty photos are used for verification and 120 are used for training. As a result of the private health information they include, the information utilised in this work are not accessible to the general public. On simple suggestion, derivation and supplemental data are accessible from the appropriate researcher.

3.2 Implementation details

With an early developmental rate of 0.0001, we used Stochastic Gradient Descent (SGD) to train the Faster R-CNN model. The system was properly trained using 40k stages, and we halted the training when the loss value reached 0.0005. On an Inspiron Lap Core i5 with 3.2 GHz computational efficiency and 8GB storage, the motivating and retaining took 48 hours. Four main forms of losses RPN regression loss, RPN detection loss, R-CNN categorization loss, and lastly R-CNN box regression loss occur throughout the training process. After every 8 steps, the model's training was routinely stored as snapshot data in meta type.

3.3 Results

The suggested technique's findings are illustrated using the identification and categorization of cracks in x-ray pictures.

Applying Modified Faster-RCNN with rotating bounding box to the long bones fractures data allows for classification and detection evaluation, as demonstrated in Figure 8. With the aid of Table 1, the predicted outcomes of the model's predictions with regard to classification are displayed in Table 2. The proposed system has attained a high level of classification accuracy. Pre-processing duration was shortened in the current study by employing the suggested technique. Table 3 displays an accuracy

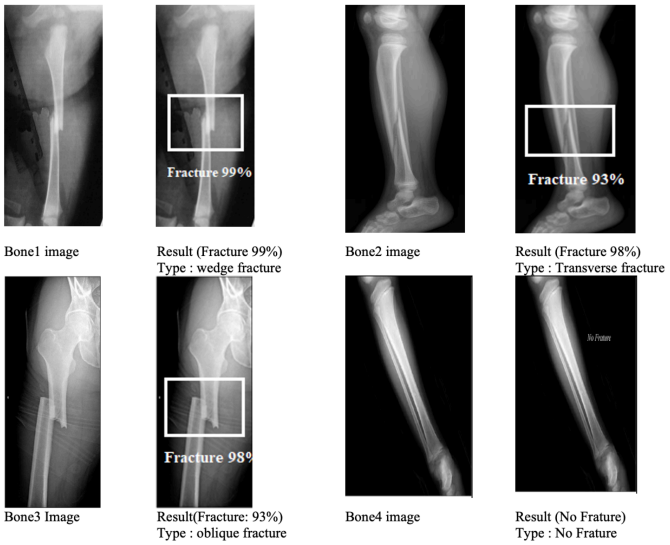

Fig 8. Model Prediction with respect to detection and classification forFracture and Non-Fracture X-Ray Images

Table 2. Prediction with Respect to Classification

S.no	Prediction	Exiting work	Proposed work
1	Sensitivity	96.7%	98.6%
2	Specificity	90.4%	92.7%
3	Precision	96.7%	98.6%
4	Accuracy	94%	96.1%
5	F1 Score	96.7%	98.6%

Table 3. Comparison with other Papers

Reference number	Year	Technique	Dataset	Accuracy
(15)	2020	Convolutional neural network (CNN)	Musculoskeletal X-Ray Images	81%
(16)	2020	Encoder-decoder structured neural network	Femur fracture in pelvic X-ray images	86.78%
(17)	2020	Convolutional neural network (CNN)	Proximal femur fracture X-Ray Image	84%
(6)	2021	Deep learning-based pertained models	Shoulder X-Ray Images	84%
(18)	2022	Models for object recognition based on deep learning	Wrist X-ray images	86%
(19)	2022	Support Vector Machine (SVM) and K-Nearest Neighbour (KNN)	Fracture Bones in X-ray Images	90%
(6)	2022	Deep Neural Networks (DNN)	X-ray pictures of broken bones	93%
Exiting work	2022	Faster R-CNN deep learning	X-ray images of long broken bones	94%
Proposed work	2022	Modified Faster R-CNN deep learning with rotated bounding box	X-ray images of long broken bones	96.1%

compared with other region studies. The main goal of this project is to use deep learning to identify and categorise long bone fractures. This method is offered to treat bone illnesses, which are also known as broken bones. It divides fractures into two categories: fractures and non-fractures. All previous techniques' performances have been contrasted and examined.

4 Conclusion

We present a new algorithm that is a modification based on the Faster R-CNN for fracture detection in X-Ray images to automatically identify and classify long bone fractures. For identifying the fracture zone and categorising it into two classes fracture and non-fracture. The modified Faster-RCNN model with rotating bounding box was implemented using a deep convolutional network architecture named VGG-16 as a foundation network. The experimental results show that the algorithm can accurately detect fracture and considerably reduce ratio of background in the bounding box. Using a bounding box, the suggested model effectively identifies long broken bone. This study can be expanded to analyse various forms of bone fractures.

References

1) Amodeo M, Abbate V, Arpaia P, Cuocolo R, Orabona GD, Murero M, et al. Transfer Learning for an Automated Detection System of Fractures in Patients with Maxillofacial Trauma. *Applied Sciences*. 2021;11(14):6293. Available from: https://www.mdpi.com/1180840.
2) Varoquaux G, Cheplygina V. Machine learning for medical imaging: methodological failures and recommendations for the future. *NPJ Digital Medicine*. 2022;5(1):1–8. Available from: https://www.nature.com/articles/s41746-022-00592-y.pdf.
3) Bengio Y, Lecun Y, Hinton G. Deep learning for AI. *Communications of the ACM*. 2021;64(7):58–65. Available from: https://doi.org/10.1145/3448250.
4) Yadav DP, Rathor S. Bone Fracture Detection and Classification using Deep Learning Approach. *2020 International Conference on Power Electronics & IoT Applications in Renewable Energy and its Control (PARC)*. 2020;p. 282–285. Available from: https://doi.org/10.1109/PARC49193.2020.236611.
5) Zhang X, Wang Y, Cheng CT, Lu L, Harrison AP, Xiao J, et al. A new window loss function for bone fracture detection and localization in X-ray images with point-based annotation. 2020. Available from: https://doi.org/10.48550/arXiv.2012.04066.
6) Hardalaç F, Uysal F, Peker O, Çiçeklidağ M, Tolunay T, Tokgöz N, et al. Fracture Detection in Wrist X-ray Images Using Deep Learning-Based Object Detection Models. *Sensors*. 2022;22(3):1285–1285. Available from: https://doi.org/10.3390/s22031285.
7) Lapeña JF, David JN, Pauig ANA, Maglaya JG, Donato EM, Roasa F, et al. Management of Isolated Mandibular Body Fractures in Adults. *Philippine Journal of Otolaryngology Head and Neck Surgery*. 2021;p. 1–43. Available from: https://doi.org/10.32412/pjohns.vi.1857.
8) Ma Y, Luo Y. Bone fracture detection through the two-stage system of Crack-Sensitive Convolutional Neural Network. *Informatics in Medicine Unlocked*. 2021;22:100452. Available from: https://doi.org/10.1016/j.imu.2020.100452.
9) Tanzi L, Vezzetti E, Moreno R, Moos S. X-Ray Bone Fracture Classification Using Deep Learning: A Baseline for Designing a Reliable Approach. *Applied Sciences*. 2020;10(4):1507. Available from: https://doi.org/10.3390/app10041507.
10) Yadav DP, Rathor S. Bone Fracture Detection and Classification using Deep Learning Approach. *2020 International Conference on Power Electronics & IoT Applications in Renewable Energy and its Control (PARC)*. 2020;p. 282–285. Available from: https://doi.org/10.1109/PARC49193.2020.236611.
11) Alzaid A, Wignall A, Dogramadzi S, Pandit H, Xie SQ. Automatic detection and classification of peri-prosthetic femur fracture. *International Journal of Computer Assisted Radiology and Surgery*. 2022;17(4):649–660. Available from: https://doi.org/10.1007/s11548-021-02552-5.
12) Ergun GB, Guney S. Classification of Canine Maturity and Bone Fracture Time Based on X-Ray Images of Long Bones. *IEEE Access*. 2021;9:109004–109011. Available from: https://doi.org/10.1109/ACCESS.2021.3101040.
13) El-Saadawy H, Tantawi M, Shedeed H, Tolba M. Bone X-Rays Classification and Abnormality Detection using Xception Network. *International Journal of Intelligent Computing and Information Sciences*. 2021;21(2):82–95. Available from: https://dx.doi.org/10.21608/ijicis.2021.79392.1101.
14) Yadav DP, Sharma A, Athithan S, Bhola A, Sharma B, Dhaou IB. Hybrid SFNet Model for Bone Fracture Detection and Classification Using ML/DL. *Sensors*. 2022;22(15):5823–5823. Available from: https://doi.org/10.3390/s22155823.
15) Kandel I, Castelli M, Popovič A. Musculoskeletal Images Classification for Detection of Fractures Using Transfer Learning. *Journal of Imaging*. 2020;6(11):127. Available from: https://www.mdpi.com/2313-433X/6/11/127/pdf.
16) Lee C, Jang J, Lee S, Kim YS, Jo HJ, Kim YS. Classification of femur fracture in pelvic X-ray images using meta-learned deep neural network. *Scientific Reports*. 2020;10(1):1–12. Available from: https://www.nature.com/articles/s41598-020-70660-4.pdf.
17) Tanzi L, Vezzetti E, Moreno R, Aprato A, Audisio A, Massè A. Hierarchical fracture classification of proximal femur X-Ray images using a multistage Deep Learning approach. *European Journal of Radiology*. 2020;133:109373. Available from: https://doi.org/10.1016/j.ejrad.2020.109373.
18) Uysal F, Hardalaç F, Peker O, Tolunay T, Tokgöz N. Classification of shoulder X-ray images with deep learning ensemble models. *Applied Sciences*. 2021;11(6):2723. Available from: https://doi.org/10.48550/arXiv.2102.00515.
19) Oyeranmi A, Ronke B, Mohammed R, Edwin A. Detection of Fracture Bones in X-ray Images Categorization. *British Journal of Mathematics & Computer Science*. 2020. Available from: https://doi.org/10.9734/JAMCS/2020/v35i430265.